PSFC/JA-10-50

ICRF Mode Conversion Flow Drive on Alcator C-Mod

Lin Y., Rice J.E., Wukitch S.J., Reinke M.L.,
Greenwald M.J., Hubbard A.E., Marmar E.S., Podpaly Y.,
Porkolab M., Tsujii N., and the Alcator C-Mod team

January 2011

Plasma Science and Fusion Center
Massachusetts Institute of Technology
Cambridge MA 02139 USA

Submitted for publication to *Nuclear Fusion*
Proceedings of 23rd IAEA Fusion Energy Conference, 2010, Daejeon, Korea.
Presentation EXW/40-1.

This work was supported by the U.S. Department of Energy, Grant No. DE-FC02-99ER54512.

ICRF Mode Conversion Flow Drive on Alcator C-Mod[1]

Y. Lin, J.E. Rice, S.J. Wukitch, M.L. Reinke, M.J. Greenwald, A.E. Hubbard, E.S. Marmar, Y. Podpaly, M. Porkolab, N. Tsujii, and the Alcator C-Mod team

Plasma Science and Fusion Center, Massachusetts Institute of Technology, Cambridge, MA, 02139, USA

e-mail contact of main author: ylin@psfc.mit.edu

Abstract We have carried out a detailed study of ICRF mode conversion flow drive on the Alcator C-Mod tokamak including its dependence on plasma and RF parameters. The flow drive efficiency is found to depend strongly on the ^{3}He concentration in D(^{3}He) plasmas, a key parameter separating the ICRF minority heating and mode conversion regimes. This result further supports the important role of mode conversion. At $+90^o$ antenna phasing (waves in co-I_p direction) and dipole phasing (waves symmetrical in both directions), we find that ΔV_0, the change in the core toroidal rotation velocity, is in the co-I_p direction, proportional to the RF power, and also increases with I_p (opposite to the $1/I_p$ intrinsic rotation scaling). The flow drive efficiency also decreases at higher plasma density and also at higher antenna frequency. The observed ΔV_0 in H-mode has been small because of the unfavorable density scaling. An empirical scaling law for $+90^o$ phasing and 180^o phasing, including L-mode and H-mode, has been obtained. At low RF power, ΔV_0 at -90^o phasing is similar to the other phasings, but at high I_p and high power, the flow drive effect appears to be saturated and to decrease vs. RF power. This observation indicates that possibly two mechanisms are involved in determining the total torque: one is RF power dependent, which generates a torque in the co-I_p direction, and the other is wave momentum dependent, i.e., the torque changes direction vs. antenna phasing. The up-down asymmetry in the mode conversion to the ion cyclotron wave may be the key to understand the flow drive mechanism.

[1] 23rd IAEA Fusion Energy Conference, presentation EXW/4-1.

1. Introduction

Plasma rotation (flow) and velocity shear can be important in stabilizing micro- and macro-instabilities in tokamak plasmas, and plasma rotation has been shown to be beneficial for tokamak plasma performance. Experimentally, sheared flow has been demonstrated to improve plasma confinement [1,2,3], and a large toroidal rotation can help stabilize MHD modes [4,5], but the issue of plasma rotation drive and control on ITER is far from being resolved. The study of plasma rotation is currently a very active research field [e.g.,6,7,8,9,10,11]. In present tokamaks, externally driven rotation is mainly from neutral beam injection as a by-product of beam heating with direct angular momentum input to the plasma. However, for ITER, the neutral beam energy will be significantly higher in order to penetrate the expected higher density plasma and larger machine size, and this requirement will result in a much lower torque per MW beam power. Beam driven rotation is thus presumed to be small in ITER. Intrinsic rotation has been observed on many tokamaks [6, 7, 11,12], and it exists independent of the external momentum input or auxiliary heating method. For ITER and future reactors, active intrinsic rotation and rotation profile control will be difficult due to its correlation to plasma pressure. Great effort has been made on present tokamaks in search of an efficient RF flow drive method that may also be applicable on ITER and beyond. A potential ITER-applicable flow drive method – ion cyclotron range of frequency (ICRF) mode conversion (MC) flow drive - has been observed on Alcator C-Mod [13,14,15,16] and also recently on JET [17,18,19]. This paper reports the results from a detailed study on Alcator C-Mod on this flow drive method.

The application of ICRF power in multiple-species tokamak plasmas, for example, D(^{3}He) plasmas, where ^{3}He is a minority and D is majority, usually involves two heating regimes: minority heating (MH) and mode conversion (MC) heating. In D(^{3}He) plasmas, when the minority concentration X[^{3}He] ($\equiv n_{3He}/n_e$) is small (e.g., a few percent on Alcator C-Mod), minority heating is dominant, where most of the launched fast magnetosonic wave (fast wave) is absorbed by the minority ^{3}He ions through the ion cyclotron (IC) resonance interaction [20]. When X[^{3}He] is larger (e.g., 10% and above), the fast wave undergoes mode conversion near the D-^{3}He hybrid layer (also called MC layer), and evolves into slower and shorter-wavelength waves: the MC ion Bernstein wave (IBW) and ion cyclotron wave (ICW) [21,22,23]. To

illustrate the difference between these two scenarios, in Figure 1 we compare the electric field of E^- contours of a minority heating and a mode conversion case from TORIC simulations. TORIC is a 2-D full wave ICRF simulation code [24,25]. The E^- field is the electric field with right-handed polarization, in the same direction as the Larmor gyration of electrons. In Figure 1-(a), at X[^{3}He] = 2%, only fast waves can be seen, and the RF power is absorbed on the ^{3}He resonance layer. In Figure 1-(b), at X[^{3}He] = 20%, near the MC layer, there are features of short wavelength waves. On the mid-plane and on the high-field-side (HFS) of the MC layer, the short-wavelength MC IBW can be identified. Above and below mid-plane, the MC ICW can be seen on the low-field-side (LFS) of the MC layer. In this MC scenario, the MC IBW is mostly absorbed by the electrons, while the MC ICW can interact with both electrons and the ^{3}He ions along its propagating path toward the LFS and to the ^{3}He IC layer. ICRF minority heating is the main heating scheme in Alcator C-Mod, but mode conversion has also been used for many interesting applications, for example, direct electron heating and sawtooth modification via local current drive [26]. Flow drive is one of the recently demonstrated applications of this ICRF heating scheme.

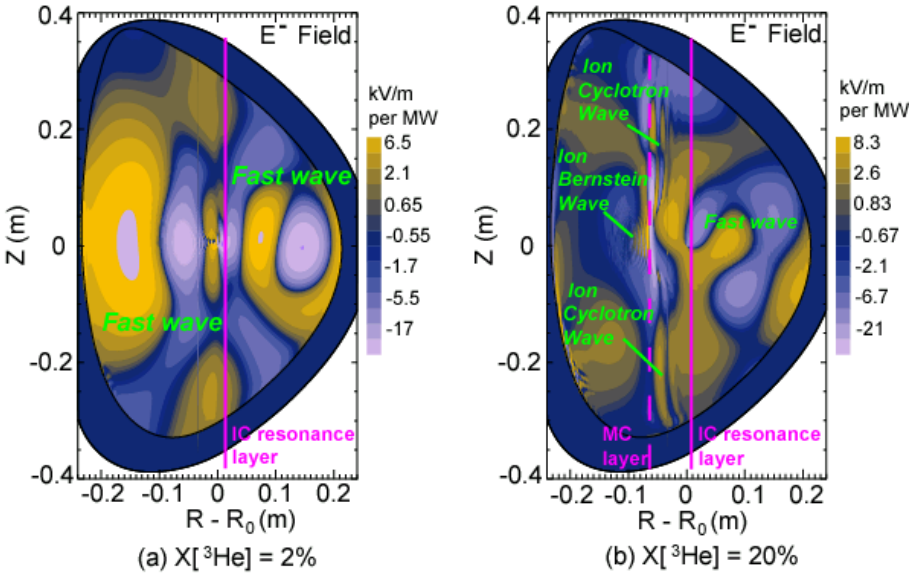

Figure 1. (Color online) Two-dimensional contours of E^- electric field (right-handed polarization) from TORIC simulations. Plasma and RF parameters: upper-single-null, B_{t0} = 5.1 T, I_p = 1 MA, f_{RF}= 50 MHz, n_ϕ = +6. (a) X[^{3}He] =2%, minority heating; (b) X[^{3}He] =20%, mode conversion heating.

Experimentally, ICRF minority heated plasmas show no evidence of direct RF driven rotation. The rotation in ICRF minority heated plasmas on Alcator C-Mod has the same trend vs. plasma stored energy and plasma current as the rotation in Ohmic plasmas [27,28]. Results from JET [29,30,31], Tore-Supra [32,33] and ASDEX-Upgrade [34] all show that the contribution of ICRF minority heating to rotation is intrinsic, i.e., not directly from the RF power absorption but rather indirectly due to the change in the plasma temperature or plasma pressure. In the previous Alcator C-Mod studies, we showed that ICRF mode conversion in D(^{3}He) L-mode plasmas can drive significantly higher plasma rotation than that from the empirical intrinsic rotation scaling. In a recent study on JET, plasma rotation driven by ICRF mode conversion has also been observed [18, 19].

In this paper, we present results from a further study of the mode conversion flow drive method on Alcator C-Mod. The experimental setup is described in Section 2. In Sections 3 to 6, we show the parametric dependence of the driven flow on a number of plasma parameters, including D(H) vs. D(^{3}He), ^{3}He concentration in D(^{3}He) plasmas, magnetic field, plasma current, plasma density, plasma shape, and confinement mode (L-mode vs. H-mode), and also dependence on RF parameters like RF power, frequency and antenna phasing. In Section 7, we show an empirical scaling law obtained from the parametric dependence study. Discussion and summary are in Section 8 and Section 9.

2. Experimental setup and main diagnostics

Alcator C-Mod [35] is a compact high field tokamak (R = 0.67 m, a = 0.22 m, $I_p \leq 2$ MA, and $B_{t0} \leq 8.1$ T). There are three ICRF antennas on Alcator C-Mod [36]. The 4-strap antenna at J-port (J-antenna) is phase variable ($+90^o$, -90^o, or 180^o) and also frequency tuneable (50 MHz, 70 MHz, or 78 MHz). It is capable of coupling ≤ 3 MW power to the plasma. The other two antennas (D-port and E-port) are operated at a fixed frequency (80.5 MHz and 80 MHz) and fixed phasing (180^o). Each of D and E antennas is capable of coupling ≤ 1.7 MW to the plasma. At $+90^o$ phasing, the launched RF wave from J-antenna is preferentially in the same direction as the plasma current (co-I_p), while -90^o phasing is counter-I_p and 180^o phasing (dipole) is toroidally symmetric. The flexibility of the antenna system and the range of toroidal magnetic field of the

tokamak provide us with a number of heating combinations (Table 1), and allow us to explore the parametric dependence of ICRF MC flow drive under multiple scenarios. In this study, we ran plasmas with toroidal field as high as 8.0 T, plasma current up to 1.35 MA, and central density n_{e0} ranging from 1 to 5 $\times 10^{20}$ m^{-3}. Central electron temperatures up to 9 keV have also been achieved via high power ICRF heating.

B_{t0}	D and E antenna (180^o phasing)	J antenna ($+90^o$, 180^o, or -90^o phasing)
~ 4 T		70 MHz, D(H) minority heating
~ 5.1 T	80 MHz, D(H) minority heating	50 MHz, D(^{3}He) mode conversion
~ 7 T		70 MHz, D(^{3}He) mode conversion
~ 8 T	80 MHz, D(^{3}He) mode conversion	78 MHz, D(^{3}He) mode conversion

Table 1 Toroidal magnetic field, antenna frequency, and ICRF heating scenarios

The mode converted waves are measured by a phase contrast imaging (PCI) system, using the heterodyne scheme as detailed in Refs [23,37]. The PCI detects the line-integrated density fluctuations induced by the ICRF waves. The spatial distribution of such fluctuations, via a synthetic diagnostic simulation based on ICRF codes like TORIC, can help us understand the ICRF physics, and reveal the possible flow drive mechanism. ^{3}He gas is puffed early in the plasma pulse, and the concentration of ^{3}He is varied by changing the duration time of the valve opening. No real-time feedback is available. The relative level of X[^{3}He] is monitored by VUV spectroscopic measurement viewing at the edge. The absolute level of X[^{3}He] is estimated and corroborated from the location of the MC waves by PCI, TORIC simulations, and the responses of temperature signals, which can be used to calculate the direct RF power deposition profile to electrons.

The plasma rotation velocity is measured by observing the Doppler shift of the H-like and He-like argon line emissions in the wavelength range of 3.7 Å -4.0 Å. A trace amount of argon is introduced by gas puffing in the early part of plasma pulses. The spectra of the line emission are obtained from a spatially resolving high resolution x-ray crystal spectrometer [38]. The instrument utilizes a spherically bent quartz crystal and a set of two-dimensional x-ray detectors to image the entire plasma cross section with a spatial resolution about 1 cm and frame rate up to 200 Hz. Observations of poloidal rotation have been reported in previous MCFD experiments

[14, 15], but unfortunately such measurements are not available in this study. The absolute value of the toroidal rotation velocity is routinely calibrated against plasmas with artificially induced locked-modes, where the rotation is presumed zero in the lab frame. The rotation velocity can also be inferred from the frequency change of the MHD modes and we can use such changes as corroborative evidence of flow drive. In Figure 2, an L-mode plasma (B_{t0} = 8.0 T, I_p = 1.2 MA, upper-single-null shape) heated with stepped-up ICRF power to 5 MW (78 MHz and 80 MHz combined) is shown. The central rotation velocity from the x-ray spectroscopy, shown in Figure 2-(a), increases from -20 km/s to 100 km/s following the step-ups of the input RF power. Positive velocity values in this paper correspond to rotation in the same direction as the plasma current (co-I_p). This observation in Figure 2-(a) is independently verified by the change of frequencies of the magnetic perturbations associated with sawtooth oscillations. The frequency changes are shown in the signals of a magnetic coil in Figure 2-(b) and those from an AXUV diode array in Figure 2-(c). The propagating velocity of these MHD modes has been studied previously and shown to approximate the plasma main ion rotation velocity near the q = 1 surface (R ~ 0.75 m for this plasma) [28]. Therefore, the frequency change up to 20 kHz shown in Figure 2-(b) and Figure 2-(c) corresponds to a plasma rotation velocity of $2\pi R \times \Delta f$ ~ 95 km/s at R ~ 0.75 m.

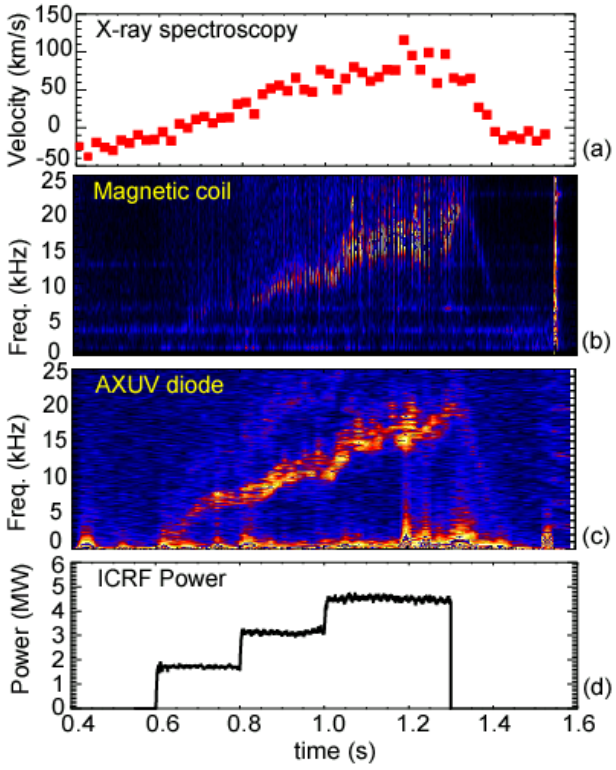

Figure 2. (Color online) (a) Central toroidal velocity from X-ray spectroscopy; (b) and (c): frequencies of magnetic perturbation from a magnetic coil and an AXUV diode; (d) Total RF power trace (78 MHz and 80 MHz). B_{t0} = 8.0 T, I_p = 1.2 MA, $n_{e0} = 1.6\times10^{20}$ m^{-3}, D(^{3}He) plasma.

The toroidal rotation profiles from the MCFD experiment are typically peaked at the magnetic axis, as shown previously in Ref. [15]. In the follow sections, we report the change of central rotation ΔV_0 and its parametric dependence, where ΔV_0 is defined as the difference of the velocity during ICRF and the velocity before the application of the RF power (Ohmic).

3. Mode conversion heating vs. minority heating

In D(^{3}He) plasmas, the concentration of ^{3}He, X[^{3}He] = n_{He3}/n_e, determines whether the fast wave launched by the antenna is heating via minority heating (MH) or mode conversion (MC) heating. A larger X[^{3}He] also moves the MC layer further away from the IC resonance layer toward the high field side. The distance between the MC layer and the IC layer strongly affects how the RF wave power is deposited. In Figure 3-(a), ΔV_0 is plotted vs. X[^{3}He] from a series of plasmas with a ^{3}He scan. All the plasmas have I_p = 0.8 MA, B_t = 5.1 T, $n_{e0} = 2.0\times10^{20}$ m^{-3}, and P_{RF} = 2.5 MW

at 50 MHz and at +90^o phasing. Figure 3-(a) shows that the maximum rotation can be obtained at X[^{3}He] ~ 10%. As shown in Figure 3-(b), in this case both the MC layer and the IC resonance are near the axis. This result suggests that an intermediate level of ^{3}He is conducive for flow drive. At low X[^{3}He], the heating scenario is ^{3}He minority heating, and at high X[^{3}He] (> 20%), the heating is mostly mode conversion electron heating. In both cases of low and high ^{3}He concentration, ΔV_0 is smaller than the intermediate ^{3}He concentration level.

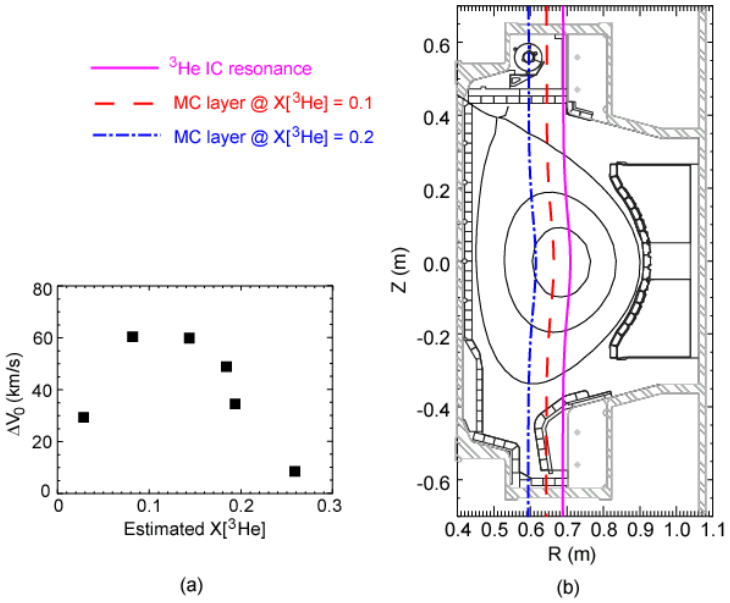

Figure 3. (Color online) Dependence of central rotation vs. X[^{3}He]. Plasma and RF parameters: B_{t0} = 5.1 T, P_{RF} = 2.7 MW, 50 MHz and +90^o phasing, n_{e0} = 2.0×10^{20} m^{-3}, I_p = 0.8 MA. (a) Change of central rotation velocity ΔV_0 vs. estimated X[^{3}He]; (b) the location of the IC resonance and MC layer at X[^{3}He] = 0.1 and 0.2.

We have also compared the rotation from the usual D(^{3}He) flow drive scenario with the routinely used D(H) minority heating scenario on Alcator C-Mod. In the D(H) heating scenario, we typically use the residual H ions for minority heating, where X[H] = n_H/n_e is nominally in the range of 4%-6%. In Figure 4-(a), we compare two L-mode upper-single-null plasmas that have the same B_t, I_p, and n_e, but one is heated with D(^{3}He) mode conversion at 50 MHz and the other one heated with the D(H) minority scenario at 80 MHz. In this setup, the H IC layer in the D(H) plasma is at the same position as the ^{3}He IC layer in the D(^{3}He) plasma. At the same RF power the D(^{3}He) MC heated plasma shows a much larger change of rotation. Two different RF frequencies were used in this comparison, and as discussed later in this paper, RF frequency may

also affect the flow drive efficiency. In Figure 4-(b), we compare two plasmas with D(^{3}He) MC and D(H) MH at the same f_{RF} = 70 MHz, but at different B fields so that they have the same IC resonance position. Again, the plasma at D(^{3}He) mode conversion shows a much larger increase in rotation. In both Figure 4-(a) and (b), the rotation velocity in the MH plasmas follows the well-established empirical $\Delta W/I_p$ scaling [27] (where W is the plasma stored energy). On the other hand, the velocity change of the MC plasmas increases vs. the level of the applied RF power. For the cases shown in Figure 4, the antenna is in +90^o phasing, and the MC flow is larger than that from the intrinsic rotation, even at smaller change in plasma stored energy.

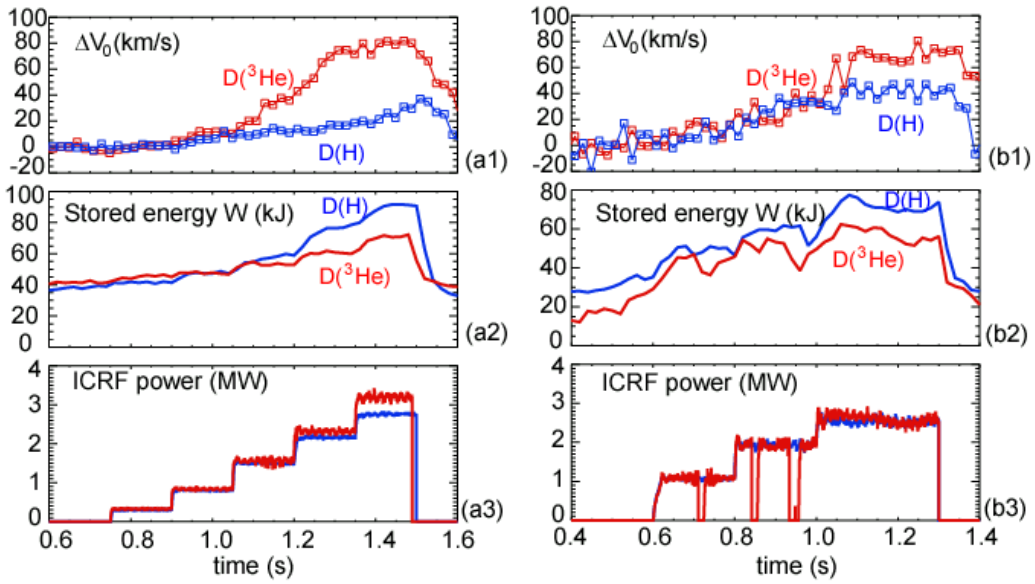

Figure 4. (Color online) Central rotation velocity, stored energy and ICRF traces. (a1-a3): B_{t0} = 5.1 T, 1.0 MA, $n_{e0} = 1.5\times10^{20}$ m^{-3}. f_{RF} = 50 MHz for D(^{3}He) and 80 MHz for D(H); (b1-b3): 70 MHz, 1.0 MA, $n_{e0} = 1.6\times10^{20}$ m^{-3}. B_{t0} = 4.6 T for D(H) and 7.2 T for D(^{3}He).

4. Dependence on RF power, plasma current and antenna phasing,

The flow drive effect is found to increase with RF power and plasma current. In Figure 5, we plot the results of plasmas at different I_p using +90^o phasing of RF power, which has four steps from 1 MW to 2.8 MW. Other parameters are B_{t0} = 5.1 T, $n_{e0} = 2.0\times10^{20}$ m^{-3}, f_{RF} = 50 MHz. The trend that ΔV_0 increases vs. P_{RF} holds for all plasma currents. For the same P_{RF}, ΔV_0 is also generally larger at larger plasma current. The I_p dependence is in the opposite direction as the intrinsic rotation observed in minority heating.

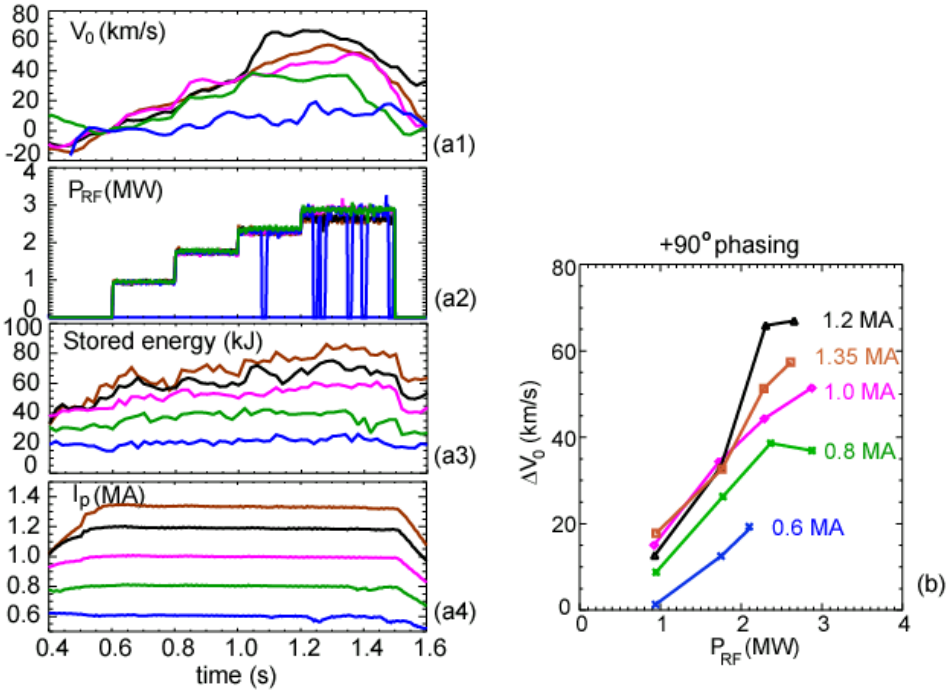

Figure 5. (Color online) central rotation vs. P_{RF} and I_p for +90° phasing. (a1-a4) V_0, P_{RF}, stored energy and I_p traces; (b) ΔV_0 vs. P_{RF} for different I_p. B_{t0} = 5.1 T, $n_{e0} = 2.0 \times 10^{20}$ m^{-3}, f_{RF} = 50 MHz.

At 180° (dipole) phasing, the net ICRF wave momentum is approximately zero, while at +90° and -90° phasings, the fast wave carries non-zero momentum. The dependence of antenna phasings has been studied in detail. In Figure 6, we show the frequency of the magnetic perturbation and rotation velocity from x-ray spectroscopy of two discharges with different antenna phasings, but otherwise identical plasma parameters (L-mode, I_p = 1.2 MA, B_{t0} = 7.9 T, $n_{e0} = 1.9\times10^{20}$ m^{-3}, and P_{RF} = 2.5 MW, f_{RF} = 78 MHz). The plasma with +90° phasing has larger rotation than that from -90° phasing. This result suggests that the antenna phasing can affect the rotation in the MC flow drive.

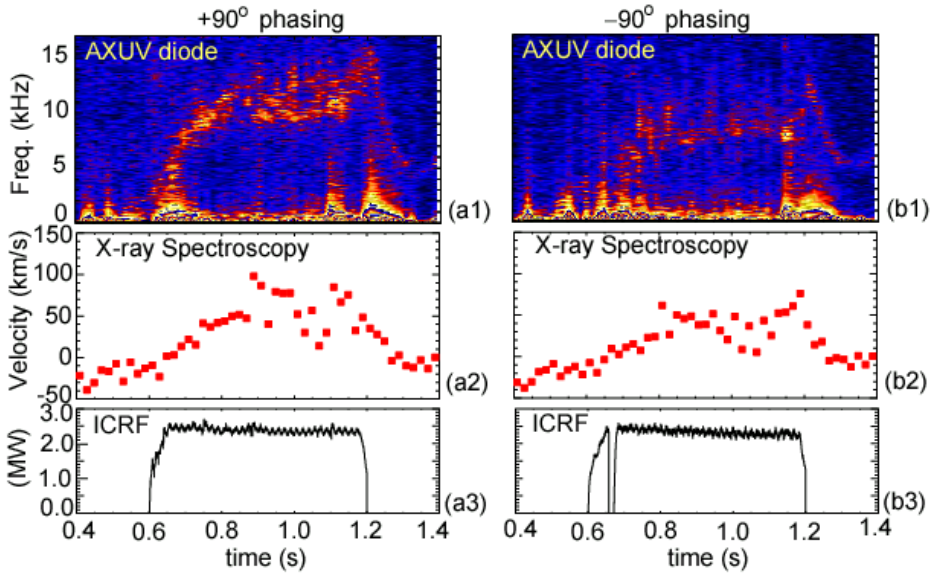

Figure 6. (Color online) Magnetic perturbation frequency, central rotation velocity and RF power traces. (a1-a3): +90° phasing; (b1-b3): -90° phasing. I_p = 1.2 MA, B_{t0} = 7.9 T, $n_{e0} = 1.9\times10^{20}$ m^{-3}, f_{RF}=78 MHz, L-mode.

Further experiments show that the effect of the antenna phasing is complicated, and I_p and P_{RF} also play a role. In Figure 7, we compare the rotation of comparable plasmas at different antenna phasings. In Figure 7-(a), the plasmas are all with I_p = 1.2 MA. We note that the rotation velocities at all three phasings are similar for P_{RF} < 2 MW, while at the higher RF power, the flow drive effect diverges: Increasing ICRF power at +90° phasing drives larger co-I_p rotation, and the rotation from dipole phasing also increases albeit at a slower rate, while at -90° phasing, the rotation actually decreases. A similar conclusion can be made from Figure 7-(b) where the flow drive effect diverges at P_{RF} > 2.3 MW for I_p = 0.8 MA.

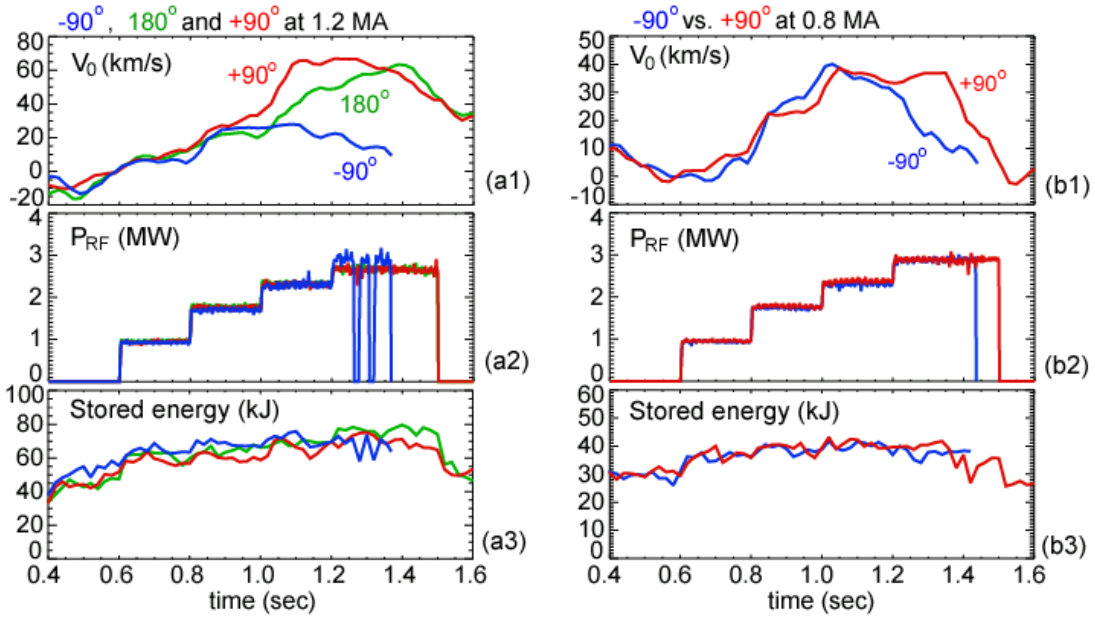

Figure 7. (Color online) Central rotation velocity, RF power, and stored energy trace vs. antenna phasing. (a1-a3) I_p = 1.2 MA; (b1-b3) I_p = 0.8 MA. B_{t0} = 5.1 T and f_{RF} = 50 MHz, $n_{e0} = 2.0\times10^{20}$ m^{-3}.

Since the fast wave carries a net counter-I_p momentum at -90° phasing and co-I_p momentum at +90° phasing, the divergence seen in the flow drive effect may be due to the difference in the wave momentum, and also suggests that the direct RF momentum input can affect the magnitude of the flow drive. Following the increase of plasma stored energy due to RF heating, the intrinsic rotation would also rise in the co-I_p direction. The observation of slowing-down rotation from the high RF power input at -90° phasing indicates that the flow drive torque might be strongly counter-I_p if there were no effect from intrinsic rotation.

5. Dependence on plasma density, L- and H-modes

The flow drive efficiency is sensitive to plasma density. In Figure 8, we show the results from a shot by shot plasma density scan of the mode conversion flow drive. All the plasmas are in L-mode, and have I_p = 1 MA, B_t = 5.1 T, P_{RF} = 2.5 MW, f_{RF} = 50 MHz and at +90° phasing. In Figure 8-(a), ΔV_0 are as high as 100 km/s at low density and as low as 20 km/s at high density. Such strong dependence on density clearly shows that lower density is favoured for the flow drive. In Figure 8-(b), the central rotation times the central density, $\Delta V_0 n_{e0}$, is plotted vs. n_{e0}. The vertical axis is approximately proportional to the total gain of the plasma angular momentum. For

$n_{e0} \leq 2 \times 10^{20}$ m^{-3}, $\Delta V_0 n_{e0}$ appears to be approximately constant vs. n_{e0}, and the rotation scaling vs. density in Figure 8-(a) is mostly likely a power (or momentum) per particle scaling. However, a precipitous drop of $\Delta V_0 n_{e0}$ at higher density indicates a more complicated mechanism.

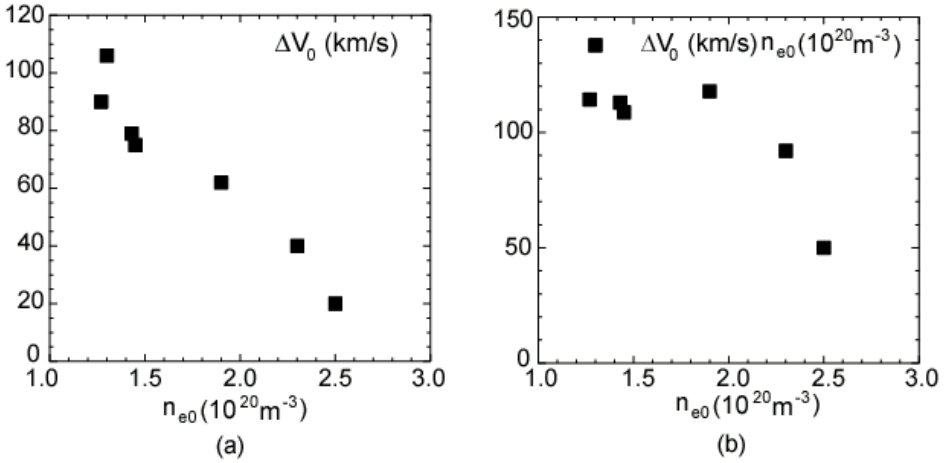

Figure 8. (Color online) Density dependence: (a) ΔV_0 vs. plasma density n_{e0}; (b) $\Delta V_0 n_{e0}$ vs. plasma density n_{e0}. Other parameters P_{RF} = 2.6 MW, f_{RF} = 50 MHz, +90° phasing, B_{t0} = 5.1 T, I_p = 1 MA.

This density scan was carried out for the upper-single-null (USN) plasmas, where the power threshold for the L-mode to H-mode transition is much higher than the typical lower-single-null (LSN) plasmas. Unlike the intrinsic rotation, the flow drive effect in LSN plasmas is shown to be very similar to that in USN plasmas for power levels below the L-H transition power threshold, thus we can rule out that plasma shape or plasma edge conditions play a significant role. Launching RF power into H-mode plasmas does not drive significant rotation in addition to the rotation arising from the intrinsic rotation. One such H-mode plasma is shown in Figure 9. In this plasma, 2 MW RF power at 80 MHz for D(H) minority heating is applied from t = 0.6 sec to 1.4 sec. The L-H transition occurs at 0.7 sec, and the plasma density shown in Figure 9-(c) and stored energy shown in Figure 9-(d) rise significantly after the transition. The rotation velocity in Figure 9-(a) also increases following the rise of the stored energy, which is typical behaviour for intrinsic rotation. At t = 0.8 sec, an additional 2.6 MW RF power at 50 MHz is applied for mode conversion flow drive. As shown in Figure 9-(d), the additional power gives the stored energy a rather large boost from ~100 kJ to ~140 kJ, but the change in the central rotation shown in Figure 9-(a) is only about 10 km/s. This weak flow drive effect in H-mode is likely due to the much higher density than that in L-mode, consistent with the results shown in Figure 8. Because it is

difficult to control H-mode density on Alcator C-Mod, we have not been able to identify the potential positive contribution to flow drive from improved momentum confinement. The obtained flow drive efficiency in H-mode appears to follow the same empirical scaling (see Section 6) as that in L-mode plasmas. Further study of flow drive in other high confinement modes having insignificant density rise, for example, the so-called I-mode [39], will help us study whether possibly better momentum confinement can improve the flow drive efficiency.

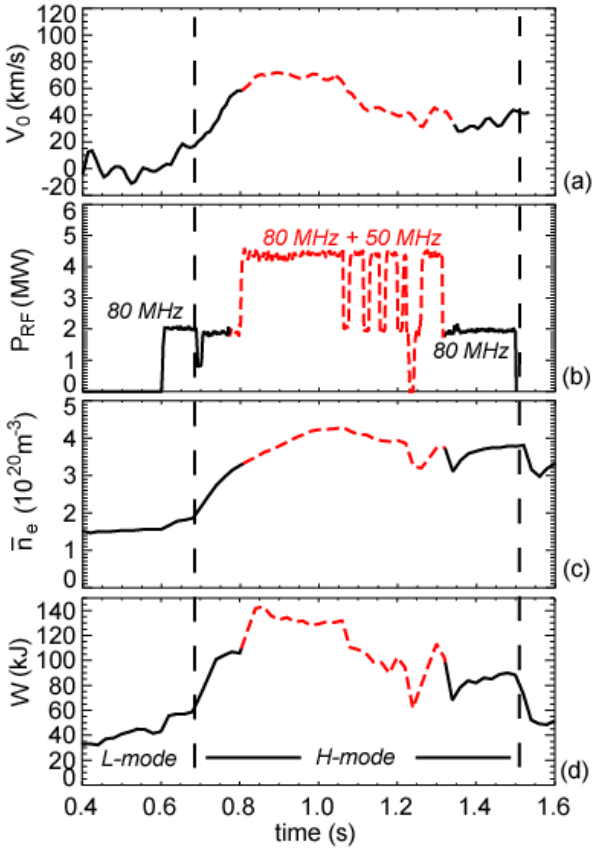

Figure 9. (Color online) Data traces in H-mode: (a) V_0; (b) P_{RF} traces. 2 MW 80 MHz power from t = 0.6 to 1.5 sec, and additional 2.6 MW/50 MHz power from t = 0.8 to 1.3 sec; (c) line averaged density; (d) stored enegy. L-mode to H-mode transition occurs at 0.7 sec. Red dashed curves indicates the time period when the 50 MHz RF power is launched for flow drive.

6. Dependence on toroidal magnetic field and RF frequency

For a fixed antenna frequency, changing the toroidal magnetic field moves the location of the MC layer and IC resonance in the plasma, and it appears to also affect the flow drive efficiency. In Figure 10, we show the result of a series of identical plasmas (I_p = 0.8 MA, $n_{e0} = 1.8\times10^{20}$ m^{-3}) at

different magnetic fields while heated with P_{RF} = 2.6 MW, f_{RF} = 50 MHz and +90^o phasing. The largest rotation is obtained for B_{t0} ~ 5.0-5.1 T as shown in Figure 10-(a). At this magnetic field, the ^{3}He cyclotron resonance is a few cm on the low field side of the magnetic axis, and the mode conversion layer (D-^{3}He hybrid layer) is also a few cm on the high field side of the axis. When both the resonance and MC layer are on one side of the plasma axis (e.g., B_{t0} = 4.5 T and 5.6 T), the flow drive is not as effective.

Similar magnetic field scans have been carried out at 70 MHz (B ~ 7 T) and 78 MHz (B ~ 8 T), and similar to the result in Figure 10, making both the MC layer and IC resonance layers close to the plasma axis is found to drive the largest central toroidal rotation. However, the flow drive efficiency at different frequencies (and magnetic field) is different even at the respectively optimized B_{t0}. In Figure 11, we show two plasmas having the same I_p = 1 MA, ^{3}He concentration, $n_{e0} = 1.4 \times 10^{20}$ m^{-3} and P_{RF} = 2.5 MW at +90^o phasing, but one is at 70 MHz/7.2 T and the other one at 50 MHz/5.1T. These two plasmas show very similar changes of plasma stored energy (and presumably similar change in intrinsic rotation), but ΔV_0 in the 50 MHz plasma, ~80 km/s, is significantly larger than that from the 70 MHz plasma, ~55 km/s. The ratio of ΔV_0 is approximately the inverse ratio of the frequencies (or equivalently, B_{t0}). Since the momentum carried by the RF waves is inversely proportional to the frequency for the same toroidal antenna structure, the dependence on RF frequency indicates the RF momentum input may play an important role in flow drive. However, we cannot simply exclude the effect of different *q* profiles of these two plasmas, which may also affect the momentum confinement and transport.

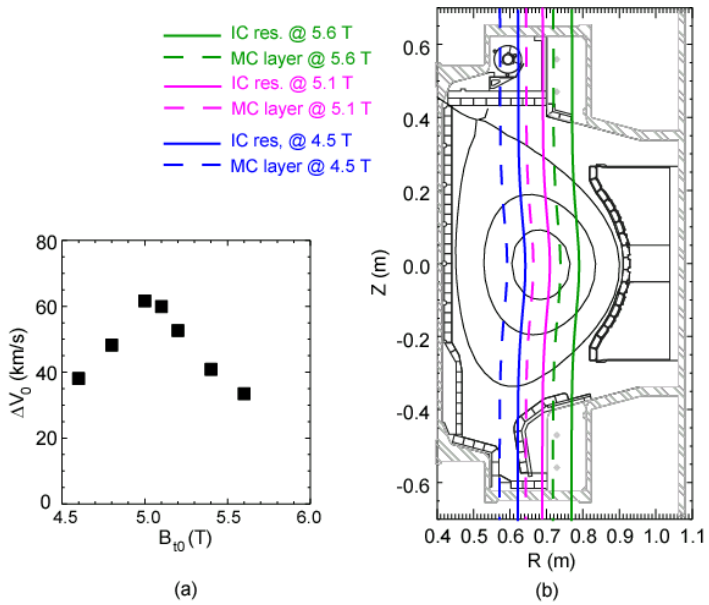

Figure 10. (Color online) B field dependence: (a) ΔV_0 vs. B field; (b) the MC layer and IC resonance locations at three B fields. I_p = 0.8 MA, n_{e0} = 1.8×10^{20}m^{-3}, P_{RF} = 2.6 MW, f_{RF} = 50 MHz and +90^o phasing.

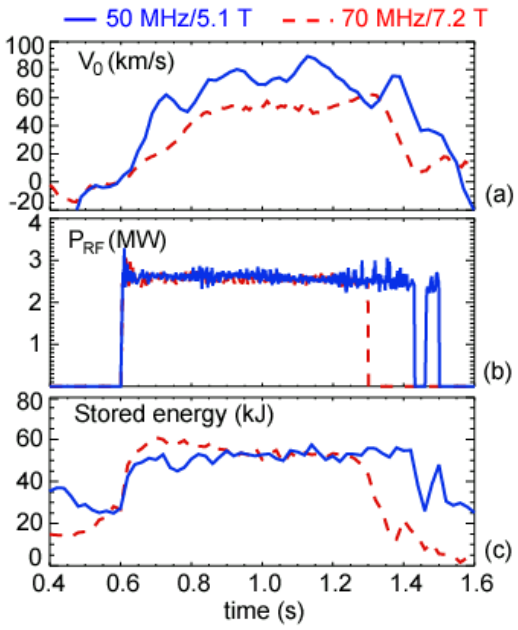

Figure 11. (Color online) Central rotation velocity at two different antenna frequencies (blue: 50 MHz and B_{t0}=5.1 T; red: 70 MHz and B_{t0} = 7.2 T): (a) V_0; (b) P_{RF}; (c) Stored energy. I_p = 1 MA, +90^o phasing, n_{eo} = 1.4×10^{20}m^{-3}.

7. Empirical scaling law of the flow drive efficiency

Our detailed experimental study has revealed the dependence of the flow drive efficiency vs. X[^{3}He], plasma current, plasma density, and RF power, frequency and antenna phasing. The result from -90^o antenna phasing is complicated, but the flow drive efficiency at +90^o and 180^o appears to have simple parametric dependences. Using all the data from dedicated experiments, we have carried out a multiple-parameter regression and obtained an empirical scaling law for the +90^o and 180^o phasings (with X[^{3}He] ~ 10% and optimal B_{t0} for chosen RF frequencies). The resulting scaling law is: $\Delta V_0[km/s] \approx 7.5\times10^2 P_{RF}[MW]^{1.3} I_p[MA]^{0.5} n_{e0}[10^{20} m^{-3}]^{-0.9} f[MHZ]^{-0.8}$. Data from different antenna frequencies and confinement modes are separately plotted in Figure 12. Note the intrinsic rotation on Alcator C-Mod (Ohmic and minority heating plasmas) approximately follows a $\Delta W/I_p$ scaling. In Figure 13, we compare the mode conversion flow drive data to the intrinsic rotation scaling. Because with RF heating the stored energy generally rises, it is no surprise that a general trend vs. ΔW exists. However, the experimental data are much more scattered to be fit with this simple $\Delta W/I_p$ scaling. While the rotation velocities from 78 MHz are not significantly different than that from this intrinsic scaling, those from 50 MHz and 70 MHz are much larger (note that both axes of the graph are logarithmic).

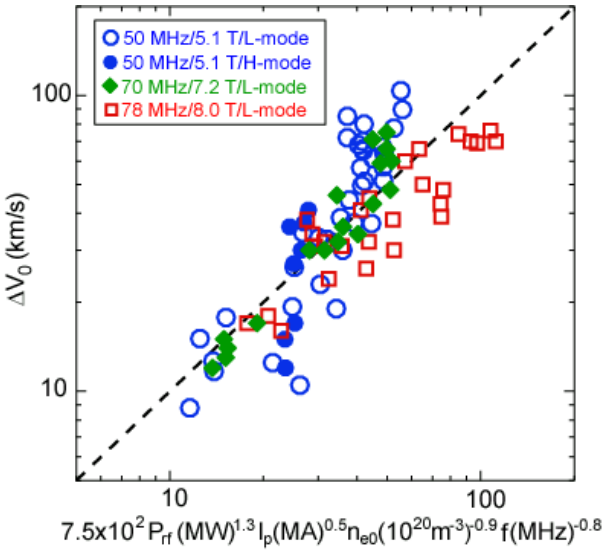

Figure 12. (Color online) Empirical scaling law for all the data from 180^o and +90^o antenna phasing. Data are grouped by antenna frequency (B field) and plasma confinement mode.

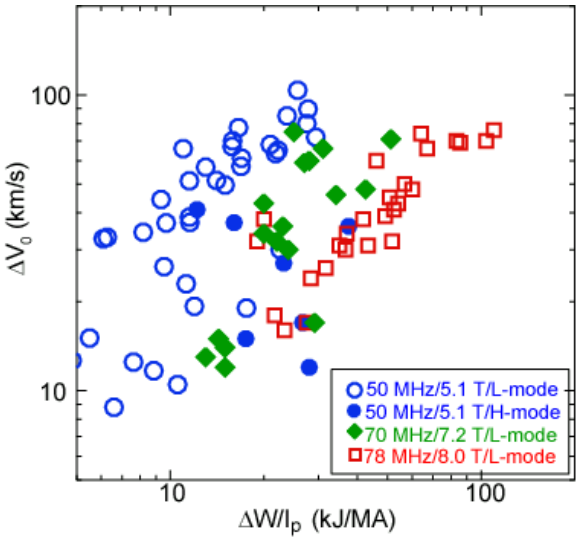

Figure 13. (Color online) MCFD rotation velocity plotted against the intrinsic rotation scaling for all the data of 180^o and +90^o antenna phasing. Same data as in Figure 12.

8. Discussion

In this study, we have determined the parametric dependence of the efficiency of mode conversion flow drive, and obtained an empirical scaling law based on the parameter scans. X[^{3}He] is one of the most important factors that determines the RF physics, whether it is in minority heating or mode conversion heating. The dependence of the rotation vs. X[^{3}He] suggests that mode conversion plays an important role. As shown in previous studies [15], in the region of intermediate X[^{3}He], the mode converted ion cyclotron waves deposits power to both ions and electrons, and we proposed that the RF power via the MC ICW to ions may be a key. Here we show some more detailed discussion on the mode conversion process and the possibility of rotation torque from this process.

In Figure 14, we show the RF power deposition to ^{3}He ions from TORIC simulation for three ^{3}He concentration levels. In Figure 14-(a), X[^{3}He] = 2% corresponds to the minority heating scenario (no mode conversion), and most ion interaction occurs with the launched fast wave on the IC resonance location. Figure 14-(b) shows the case of X[^{3}He] = 10%. In this case, some RF power to ions via the fast wave is apparent, but there is also a significant amount to ions via the MC ICW above and below mid-plane. In Figure 14-(c), in the case of X[^{3}He] = 20%, there is some

power to ions via FW and the MC ICW, but the total level is much smaller. Note all the three plots have the same logarithmic color scale. Experimentally, we have observed that the scenario of Figure 14-(b) has the most flow drive effect. In Figure 15, the RF power to ions via the MC ICW is plotted vs. X[^{3}He]. This result is obtained from a single toroidal mode, $n_\phi = +6$, the peak antenna spectrum. As a result, the trend is only qualitative. Interestingly, the peak in the figure is rather similar to Figure 3.

The mode conversion to the ICW is up-down asymmetric. This can be clearly seen in the power deposition contours in Figure 14-(b) and (c) and it can also be seen in the field contours of Figure 1-(b). Because of the requirement of an up-shift of $k_\parallel$ for the MC ICW to exist, the waves above and below the mid-plane have different wavelengths (opposite sign of $k_\parallel$) and they are generally at different vertical locations and flux surfaces. A detailed description and experimental study of this up-down asymmetry can be found in Ref. [37]. Although the total canonical momentum of the system, RF waves and plasma, is conserved, the mode converted waves have larger momentum content per MW than the launched fast wave, by gaining momentum via non-resonance process [40]. The MC ICWs then carry the momentum to differential spatial locations, and deposit their momentum to ions via the ion cyclotron resonance interaction. A detailed mechanism that may convert this asymmetry to plasma rotation needs more theoretical and experimental work.

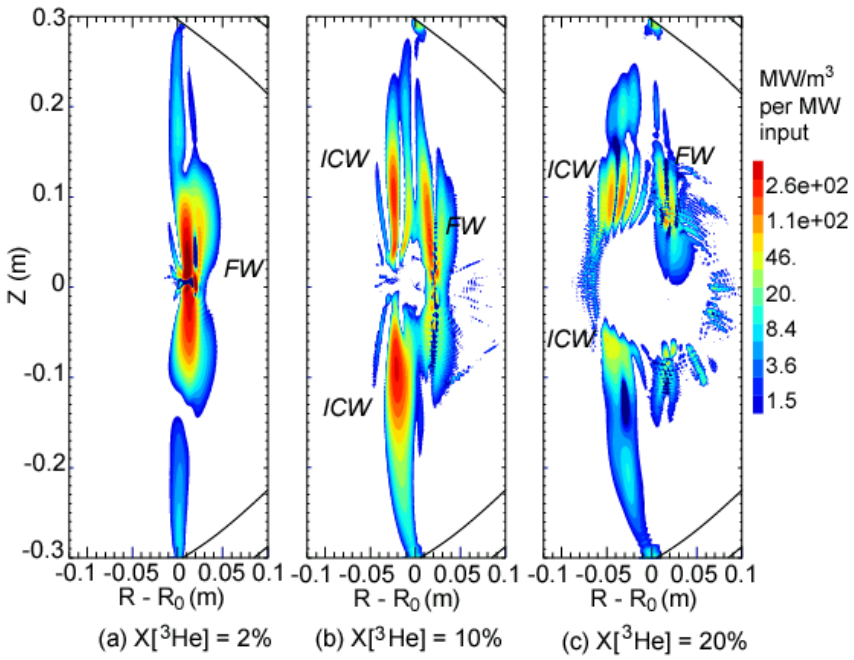

Figure 14. (Color online) Power deposition to ^{3}He ions from TORIC simulations. (a) X[^{3}He] = 2%; (b) X[^{3}He] = 10%; (c) X[^{3}He] = 20%. B_{t0} = 5.1 T, RF frequency = 50 MHz, I_p = 1.0 MA, n_{e0} = 2.0 × 10^{20} m^{-3}. Toroidal mode number in the simulation n_ϕ = +6.

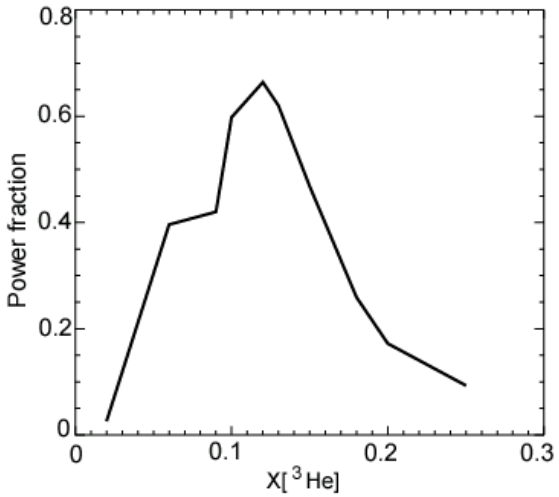

Figure 15. (Color online) RF power to ^{3}He ions via the MC ICW vs. X[^{3}He] from TORIC simulations. Same parameters as those in Figure 14.

The empirical scaling law of MC flow drive, approximately $P_{rf}\sqrt{I_p}/n_e f$, indicates that the ICRF power (or momentum) per particle plays an important role. The positive dependence on I_p may suggest a momentum confinement scaling (similar to energy scaling). In addition, I_p can also affect the mode conversion to the ion cyclotron wave by varying the poloidal magnetic field. The interaction between the mode converted ion cyclotron waves and the ^{3}He ions, and its associated

momentum asymmetry has been thought to be the key to generate the flow [14, 15, 19]. The experimental observation for $+90^o$ phasing is consistent with this conjecture. But the complicated P_{RF} and I_p dependence for -90^o antenna phasing indicates that possibly two mechanisms are involved in determining the total torque: one is RF power dependent (i.e., independent of the antenna phasing), which generates a torque in the co-I_p direction on Alcator C-Mod; the other is wave momentum dependent, i.e., the torque changes direction vs. antenna phasing. Other plasma parameters, like I_p and n_e, can affect both the mode conversion process and momentum confinement and transport. The density effect on mode conversion is complicated, for example, Ref. [41]. And the approximately inverse density scaling in the empirical scaling law indicates that the power or momentum per particle is the dominant role played by the density. The steep drop off of the flow drive effect at very high density in L-mode (Figure 8) and in H-mode (Figure 9) is not yet understood. Larger plasma current generally increases the total power to the MC ICW by introducing larger poloidal field, and it also affects the momentum confinement. This is consistent to the experimental observations.

The intrinsic rotation, which exists independent of RF heating, is complicating our study. All the rotation changes presented above are a combination of the change in intrinsic rotation and presumably RF driven rotation. The scaling law shown in Figure 12 refers to this combined effect. Experimentally, we have not been able to separate these two types of rotation. We have also performed a multi-parameter regression by excluding the intrinsic rotation in the data using the simple $\Delta W/I_p$ empirical law, but this approach has failed to produce a meaningfully better scaling law mainly because the intrinsic rotation values are very scattered.

9. Summary

ICRF mode conversion flow drive has been studied in detail on Alcator C-Mod. The flow drive efficiency has been shown to depend on the ICRF power, frequency, and antenna phasing, the level of ^{3}He concentration in D(^{3}He) plasmas, plasma density, plasma current, and magnetic field. An empirical scaling law has been obtained for the $+90^o$ phasing and dipole phasing. At -90^o phasing, the parametric dependence is more complicated, and in general, the co-I_p rotation

velocity is smaller. The experimental evidence suggests that both the ICRF heating and momentum carried by the wave play roles in driving the flow, and the asymmetry associated with the mode conversion process may be the key to understand the flow drive mechanism.

Acknowledgments

The authors thank the Alcator C-Mod operation and ICRF groups. This work was supported at MIT by U.S. DoE Cooperative Agreement No. DE-FC02-99ER54512. Computer simulations using TORIC code were carried out on the MIT PSFC parallel AMD Opteron/Infiniband cluster Loki.

References

[1] Burrell K.H. 1997 *Phys. Plasmas* **4** 1499

[2] Politzer P.A. *et al* 2008 *Nucl. Fusion* **48** 075001

[3] Mantica P. *et al* 2009 *Phys. Rev. Lett.* **102** 175002

[4] Strait E.J. *et al* 1995 *Phys. Rev. Lett.* **74** 2483

[5] Garofalo A.M. *et al* 2001 *Nucl. Fusion* **41** 1171

[6] Rice J.E. *et al* 2007 *Nucl. Fusion* **47** 1618

[7] deGrassie J.S. *et al* 2009 *Plasma Phys. Control. Fusion* **51** 124047

[8] Tala T. *et al* 2009 *Phys. Rev. Lett.* **102** 075001

[9] Rice J. *et al* 2009 *Nucl. Fusion* **49** 025004

[10] Yoshida M. *et al* 2009 *Phys. Rev. Lett.* **103** 065003

[11] Solomon W. *et al* 2010 *Phys. Plasmas* **17** 056108

[12] Bortolon A. *et al* 2006 *Phys. Rev. Lett.* **97** 235003

[13] Lin Y., *et al 22nd IAEA Fusion Energy Conference,* Geneva, Switzerland (2008) PD1- 2

[14] Lin Y., *et al* 2008 *Phys. Rev. Lett.* **101** 235002

[15] Lin Y., *et al* 2009 *Phys. Plasmas* **16** 056102

[16] Rice J.E., *et al 37th EPS conference on Plasma Physics* (Dublin, Ireland, 21-25 June, 2010).

[17] Tala T., *et al 23rd IAEA Fusion Energy Conference,* Daejeon, Korea (2010) EX3-1

[18] Lin Y., *et al 37th EPS Conf. on Plasma Physics and Controlled Fusion* (Dublin, Ireland, June 2010).

[19] Lin Y., *et al* "ICRF mode conversion flow drive in D(^{3}He) plasmas on JET", *to be submitted to Plasma Phys. Control. Fusion*

[20]Porkolab M. 1994 Plasma heating by fast magnetosonic waves in tokamaks, N. Fisch ed. *Advances in Plasma Physics, AIP Conference Proceedings.* Vol **304** p99

[21] Perkins F.W. 1977 *Nucl. Fusion* **17** 1197

[22] Adams J. 1987 *Plasma Phys. Control. Fusion* **29** 443

[23] Nelson-Melby E. *et al* 2003 *Phys. Rev. Lett.* **90** 155004

[24] Brambilla M. 1999 *Plasma Phys. Control. Fusion* **41**

[25] Wright J. C. *et al* 2004 *Phys. Plasmas* **11** 2473

[26] Parisot A. *et al* 2007 *Plasma Phys. Control. Fusion* **49** 219

[27] Rice J.E. *et al* 1999 *Nucl. Fusion* **39** 1175

[28] Hutchinson I.H. *et al* 2000 *Phys. Rev. Lett.* **84** 3330

[29] Eriksson L.-G., *et al* 1997 *Plasma Phys. Control. Fusion* **39** 27

[30] Eriksson L.-G., *et al* 2009 *Plasma Phys. Control. Fusion* **51** 044008

[31] Noterdaeme J. M., *et al* 2003 *Nucl. Fusion* **43** 274

[32] Assas S. *et al 30th EPS Conf. on Plasma Physics and Controlled Fusion* (St Petersburg, Russia, 7-11 July 2003) ECA **27A,** P-1

[33] Eriksson L.-G. *et al* 2001 *Nucl. Fusion* **41** 91

[34] Assas S. *et al* 2007 *Radio Frequency Power in Plasmas,* edited by P.M. Ryan and D. A. Rasmussen, *AIP Conference Proceedings* **978** 103

[35] Marmar E. S., *et al* 2007 *Fusion Sci. Tech.* **51**, Alcator C-Mod special issue.

[36] Bonoli P., *et al* 2007 *Fusion Sci. Tech.* **51** 401

[37] Lin Y. *et al* 2005 *Plasma Phys. Control. Fusion* **47** 1207

[38] Ince-Cushman A. *et al* 2008 *Rev. Sci. Instrum.* **79** 10E302

[39] Whyte D. *et al* 2010 *Nucl. Fusion* **50**, 105005.

[40] Hellsten T. 2009 *16th Topical Conf. on RF Power in Plasmas (Gent, Belgium, 2009) AIP Conference Proceedings* **1187** P625

[41] van Eester D. *et al* 2009 *Plasma Phys. Control. Fusion* **51** 044007